Available online at www.sciencedirect.com

ScienceDirect

Geochimica et Cosmochimica Acta 284 (2020) 61–74

Geochimica et Cosmochimica Acta

www.elsevier.com/locate/gca

Rapid post-mortem oxygen isotope exchange in biogenic silica

Shaun P. Akse, Jack J. Middelburg, Helen E. King, Lubos Polerecky

Department of Earth Sciences, Utrecht University, PO Box 80021, 3508 TA Utrecht, the Netherlands

Received 24 March 2020; accepted in revised form 7 June 2020; available online 18 June 2020

Abstract

The oxygen isotope composition of diatom frustules is thought to reflect the isotopic composition of the ambient seawater at the time of biomineralisation. However, significant concerns exist surrounding the degree of post-mortem alteration that might occur. Here, we study post-mortem overprinting of the $\delta^{18}O$ signal in various forms of silica by incubating the samples in ^{18}O-enriched seawater and analysing them with nanoSIMS and Raman micro-spectroscopy. The nanoSIMS data show that significant ^{18}O-exchange occurs throughout diatom frustules (fresh as well as fossil) over days to weeks when placed in ^{18}O-enriched seawater. This is a time-scale similar to that of the sinking diatom detritus in marine systems. Similarly, rapid ^{18}O-exchange, although to a lesser degree, also occurs in sponge spicules. In contrast, no significant ^{18}O-exchange occurs on this time-scale in crystalline silica, most likely due to the absence of silanol (Si-OH) groups as observed in Raman measurements. Together these results confirm that the oxygen signature of external silanol groups can be overprinted on short timescales, but also show that internal silanol groups are similarly susceptible. These internal silanols form a large pool of oxygen in the silica structure and are difficult to remove when cleaning. This results in the presence of an internal pool directly influenced by changes in the external water signature which may potentially be incorporated into the silica structure during maturation. The final measured $\delta^{18}O$ in biogenic silica, therefore, most likely, represents a mixture of signals from the original growing stage, water-column settling, and sediment pore waters.

Keywords: Biogenic silica; Oxygen; Isotope; Maturation; NanoSIMS; Raman spectroscopy; Paleoclimatology

1. INTRODUCTION

The oxygen isotopic composition of past waters is considered an important paleoceanographic tool, because it provides information on past temperature, changes in global ice volume and regional processes impacting seawater salinity (e.g., Rohling and Cooke, 1999; Swann and Leng, 2009). Measuring $\delta^{18}O$ in foraminiferal shells is a commonly used method to track changes in the $\delta^{18}O$ of ambient water during growth (e.g., Zachos et al., 2001). Unfortunately, foraminifera and other carbonate remains are not always well preserved on the ocean floor, impeding our knowledge of paleoceanographic conditions in the geological past. Therefore, in areas where carbonates are absent, other forms of biogenic material are required to study the changes in seawater $\delta^{18}O$ over time. One material that could help fill the gaps in the record is biogenic silica (opal), which is predominantly represented in the sedimentary record by diatom frustules, radiolaria skeletons and sponge spicules.

As for most silicates, diatom silica is composed mainly of interlinked silica (SiO_4) tetrahedrons. These units connect via bridging oxygen atoms forming siloxane (–Si-O-Si–) bonds (Zhuravlev, 2000). Formation of biogenic silica occurs via condensation reactions, where two Si-OH groups on the silicic acid units condense to form $SiO_2 + H_2O$. The $\delta^{18}O$ of the resulting biogenic SiO_2 is assumed to reflect the $\delta^{18}O$ and temperature of the water in which it formed. The tetrahedrally bonded –Si-O-Si is

E-mail addresses: s.p.akse@uu.nl, shaun.akse@gmail.com (S.P. Akse), J.B.M.Middelburg@uu.nl (J.J. Middelburg)

https://doi.org/10.1016/j.gca.2020.06.007
0016-7037/

surrounded by a less dense hydrous layer consisting of –Si-OH groups (silanols) (Gendron-Badou et al., 2003). Silanols can be present on the surface of the frustule (external) or trapped in the porous structure as internal silanols (Loucaides et al., 2010; Zhuravlev, 2000). Moreover, the oxygen atom in the silanols is thought to continuously exchange with the oxygen atom in the surrounding water molecules (e.g. Labeyrie and Juillet, 1982). The question remains whether both external and internal silanols are equally affected by secondary oxygen signal overprinting, and whether this has consequences for the tetrahedrally bonded oxygen. If this were the case, $\delta^{18}O_{diatom}$ values would most likely be similar to those in the ambient water during biomineralization, but may start to deviate from this signal post-mortem.

Most studies on biogenic silica focus on either diatoms (unicellular primary producers) or sponges. Siliceous sponges, predominantly from the classes *Demospongiae* and *Hexactinellida*, produce spicules (structural elements that support the skeleton of the animals). Sponge spicules have an amorphous silica matrix similar to that of diatom frustules (Gendron-Badou et al., 2003; Sandford, 2003), but differ in their formation processes as well as their physical characteristics. While diatom frustules are known for their large structural pores, sponge spicules are often observed to have concentrically layered, needle-like structures with a single hollow central core (axial canal) (Müller et al., 2007). Additionally, the two groups of organisms represent different environmental conditions: while diatoms live predominantly in the surface waters, sponges are benthic organisms and thus live in the bottom waters. This combination of similarities and differences provides the potential to reconstruct not only surface and bottom water $\delta^{18}O$, but also vertical gradients in $\delta^{18}O$ (e.g. Snelling et al., 2014).

In recent decades, the application of oxygen isotopes in fossil diatom frustules has become an increasingly popular tool for reconstructing past climate and environmental changes, both in lacustrine and marine settings (see Leng and Barker, 2006; Swann et al., 2006; Swann and Leng, 2009). Despite increasing interest in this proxy, the presence of silanol groups in the silica matrix and their susceptibility to post-mortem isotopic overprinting remain a point of concern. These concerns are strengthened by observed differences in $\delta^{18}O_{diatom}$ between living diatoms and diatoms taken from deep-water traps and surface sediments. This disparity is particularly evident in the vast array of calculated silica-water fractionation factors (fresh/recent: Brandriss et al., 1998; Dodd and Sharp 2010; sedimentary: e.g., Juillet-Leclerc and Labeyrie, 1987; Matheney and Knauth, 1989; Shemesh et al., 1992). Finding the source of this variability is essential for reliable application of this proxy, and studying the variability on an individual frustule level may aid this search.

Meanwhile, the use of oxygen isotope analysis in spicules is rare, as studies have suggested that the fractionation between sponge spicules and seawater is not systematically reliable, despite some studies showing clear trends in $\delta^{18}O$ (Matheney and Knauth, 1989; Matteuzzo et al., 2013; Snelling et al., 2014, Hendry et al., 2015). Instead, the study of sponge spicules as a paleoproxy has focused on silicon isotopes (e.g., Hendry et al., 2010; Hendry and Robinson, 2012).

With this knowledge, it becomes clear that, in order to analyse the potential of $\delta^{18}O$ in biogenic silica as a paleoproxy tool, the driving mechanisms behind the observed variability need to be studied further. Recent studies regarding post-mortem diatom frustule maturation have focused predominantly on diagenesis occurring in the sediments, assuming that no exchange of oxygen occurs during the settling of diatom detritus through the water column. This assumption is based on the presence of an organic membrane surrounding the frustule, which protects it from dissolution (Bidle and Azam, 1999; Bidle et al., 2003) and appears to inhibit post-mortem changes in $\delta^{18}O$ (Moschen et al., 2006). In the sediments, several processes may influence the silanol groups and may thus induce isotopic exchange. A study on dissolution effects in sedimentary frustules suggests that small changes in $\delta^{18}O_{diatom}$ can be observed in a state of extreme dissolution (Smith et al., 2016). Other proposed processes are the precipitation of secondary silica and addition of silanol groups, and the condensation of silica (Schmidt et al., 2001; Dodd et al., 2012, 2017; Moschen et al., 2006). The effect of silica condensation on $\delta^{18}O$ was studied by ageing cultured diatoms in a setting mimicking seafloor/sedimentary conditions (Dodd et al., 2017), which revealed rapid and significant changes in $\delta^{18}O$ coinciding with a reduction in the total silanol abundance. Moreover, the silica-water fractionation relationship factor in the experimentally aged samples approached equilibrium quartz-water fractionation. Because of this, it was suggested that silica-water fractionation relationships derived from coretop/shallow sedimentary silica may represent a mixed signal from $\delta^{18}O$ values acquired during growth and diagenetic hydroxylation. Furthermore, it was suggested that, despite the decreasing reactivity, this process is likely to continue for about $10^4 - 10^6$ years, possibly resulting in complete isotopic re-equilibration of the oxygen isotopes (Dodd et al., 2017).

To reduce the role that exchangeable oxygen in silanol groups can have in determining the $\delta^{18}O_{diatom}$, several analytical methods have been developed. Two main methods have been established and compared in an inter-laboratory study: the controlled isotope exchange (CIE) method and the stepwise fluorination (SWF) method (Chapligin et al., 2011). Both analytical methods were shown to produce comparable and reproducible results demonstrating that the observed mismatch is not due to the analysis method. Recent studies, however, suggest that sample preparation and laboratory protocols can have significant effects on the measured $\delta^{18}O_{diatom}$ (Menicucci et al., 2017; Tyler et al., 2017), reviving concerns about the effectivity of the current methods in removing post-mortem $\delta^{18}O_{diatom}$ signals.

In this study, we challenge the assumption that water-column maturation plays a marginal role in controlling $\delta^{18}O$ in biogenic silica. NanoSIMS analysis of post-mortem ^{18}O enrichment in fresh diatom detritus and siliceous sponge spicules incubated in ^{18}O-enriched seawater reveals a rapid and homogenous signal overprinting, which

is absent in crystalline silica. When combining the imaging data from the nanoSIMS with structural data from Raman analysis, the results suggest that oxygen exchange not only occurs in the surface silanol groups, but similarly in the internal silanol groups, which potentially alter the final $\delta^{18}O$ signature of the silica.

2. MATERIALS & METHODS

2.1. Materials

Two separate centric diatom batches were cultured (*Thalassiosira pseudonana* and *Thalassiosira weisflogii*) at the Royal Netherlands Institute for Sea Research (NIOZ) by using f/2 medium based on natural seawater (NSW). The culture collection of the NIOZ provided the *T. weisflogii* strain (CCAP 1085/18) while the *T. pseudonana* strain (CCAP 1085/12) was acquired at the Culture Collection of Algae and Protozoans (CCAP) in Scotland. Cultures were grown in 300 cm^3 tissue culture flasks at a temperature of 20 °C under a 16 h/8h light/dark cycle. A total of 2 L of medium per diatom species was produced and split into 500 mL containers for harvesting. After harvesting, the diatoms were killed by freeze-drying (Telstar LyoQuest) and stored at −20 °C. An aliquot of each 500 mL container was taken for cell counts determination using flow cytometry (data not shown). Before use, freeze-dried samples were diluted with 50 mL of MilliQ (18.2 MΩ·cm at 25 °C). Frustule diameters ranged between 4 and 10 μm.

The sponge spicule sample (*Vazella pourtalesi*) was provided by M. C. Bart (Amsterdam University). The *Hexactinellida* class sponge specimens were collected attached to their rocky substrate by the ROPOS ROV at 300 m depth during the Hudson cruise 2016–019 (September 2016) at the Emerald Basin (43°59′49.0″ N, 62°46′15.7″ W). Spicule diameters generally ranged between 10–20 μm.

The quartz crystals were provided by A. Roepert (Utrecht University). The crystals were collected near Al Hajar, Oman (23°20′25.0″ N, 58°33′57.0″ E) from a quartz vein permeating a Late Proterozoic phyllite. Age of the crystals has not been determined. The crystals were crushed resulting in particle sizes of 50–150 μm. The sand grains used in this study originate from standard construction-grade sand, with targeted grain size between 60–100 μm .

Fossil frustules were provided by Henko de Stigter (NIOZ). They originate from the 40–60 μm size fraction of a diatomaceous clay collected in the Peru basin (07°04.4′ S, 088°27.8′ W) at 4150 m water depth during the summer of 2015. This sediment was the remainder of a boxcore after the top 20 cm had been removed; the fossil frustules thus have an age more than 10,000 years (Akse, 2020a, 2020b).

2.2. Incubation experiments

Two types of incubation experiments were performed in this study. Most experiments had multiple time-points to study the exchange dynamics of different materials. One experiment had only one time-point, but was performed at two temperatures.

Similar set-ups were used for the incubation experiments with the biogenic silica (diatom frustules and sponge spicules) and the crystalline silica (quartz crystals and sand grains) samples. Incubations were done in 1.5 mL Eppendorf tubes containing 1.1 mL of ^{18}O-labeled water (^{18}O atom fraction of 9%) prepared by mixing 0.1 mL of 97% $H_2^{18}O$ (Sigma-Aldrich) with 1 mL of unlabeled natural seawater water (NSW) from the North Sea. Control incubations only used unlabeled NSW. For the experiments, material from each sample was added to separate tubes. The Eppendorf tubes were put into Greiner tubes and placed in a horizontal position on a roller-table to keep the water moving and the material in suspension. Additional experiment-specific details are given below.

For half of the diatom ^{18}O-labeled incubations, the NSW was autoclaved before the ^{18}O-label was added, whereas for the other half the ^{18}O-label was added to NSW. This was done to assess the role of microbial degradation on the protective organic layer surrounding the frustule (Bidle and Azam, 1999; Bidle et al., 2003). No autoclaving was done for the control incubation. Diatoms (mixture of *T. pseudonana* & *T. weisflogii*) were added to the incubation seawater in 0.01 mL aliquots (resulting in ~10^5 cells per tube). For the time-series study, the diatoms were kept in solution for 0.5 h, 1 h, 24 h, 168 h (1 week), 336 h (2 weeks), 672 h (4 weeks), and 1008 h (6 weeks), and incubated in a climate-controlled room at 15 °C.

To test for temperature dependence, additional diatom incubations were performed at 4 °C (bottom-water conditions) and 15 °C (surface-water conditions) for 336 h. The same diatom mixture was used. As the frozen diatom samples had already been diluted with MilliQ, these diatoms were suspended in solution for an extended period compared to the previously mentioned experiments, resulting in higher initial dissolved silica (DSi) concentrations.

To test the impact of diagenesis on ^{18}O exchange, fossil diatom frustules were incubated in ^{18}O-enriched NSW and unlabeled NSW (control) for 336 h (Akse, 2020a, 2020b). For this experiment, a batch of the acquired diatomaceous clay sediment (see materials) and a beaker of natural seawater were placed in a glovebox for over 24 hours in order to simulate anoxic bottom water conditions, and then mixed. For the mixing, the sediment–water ratio was kept at a 1:1 volume ratio. A 1.5 mL Eppendorf vial was filled with 0.5 mL of the sediment–water mixture. Each sample tube was topped with 1.1 mL of the ^{18}O enriched NSW. The samples remained under anoxic conditions during the incubation period (336 h).

The sponge spicules received a similar treatment to the diatoms. However, only spicules incubated for 24 h and 336 h (2 weeks), and a control sample incubated in NSW for less than 1 h, were analyzed. The quartz crystals and sand grain samples were only studied after 336 h (2 weeks) of incubation in the ^{18}O-enriched NSW and in unlabeled NSW (controls).

At the end of the incubation, the samples were centrifuged for 10 min (RCF = 15411 g, 20 °C) to settle the

material. Supernatant (1 mL) was extracted and filtered through a sterile 0.2 μm VWR syringe-filter for dissolved silicate determination (Fig. S1). The remaining material was rinsed with autoclaved MilliQ and filtered onto a 0.2 μm Nuclepore polycarbonate (PC) filter. The filter was then air-dried and stored in a Petri dish at 15 °C.

To check for potential changes in the $\delta^{18}O$ of the water during incubation, the supernatant for two diatom samples (time-points 1 h and 336 h) was analyzed using OA-ICOS (LGR Off-Axis Integrated Cavity Output Spectroscopy). No significant change in $\delta^{18}O_{water}$ was detected ($\delta^{18}O_{1h} = 32.61 \pm 0.52$(SD); $\delta^{18}O_{336h} = 32.94 \pm 0.46$(SD), $n = 3$).

2.3. NanoSIMS measurements and data processing

Nano-scale secondary ion mass spectrometry (nanoSIMS) was used to quantify ^{18}O atom fractions in individual specimens of diatom frustules, sponge spicules and crystalline silica. Sample preparation varied among the different sample types due to their different morphological properties (see details in Supplementary Methods). Before the measurements, samples were placed in a vacuum to remove any adsorbed water. This included the airlock of the NanoSIMS instrument (10^{-8} mbar), where they remained for at least 24 h at ~50 °C, and the vessel chamber (10^{-9} mbar), where they were kept until analysis (20 °C, minimal of 3 days).

NanoSIMS measurements were performed with the NanoSIMS 50L instrument (Cameca, France) operated at Utrecht University (see Nuñez et al. (2018) for a review of the method). Electron multiplier detectors were set using a standard (SPI Supplies, 02757-AB 59 Metals & Minerals Standard) to enable the detection of secondary ions $^{12}C^-$, $^{16}O^-$, $^{18}O^-$, $^{12}C^{14}N^-$, $^{28}Si^-$ and $^{32}S^-$ with the Cs^+ primary ion beam. This study focused predominantly on the oxygen isotopes, but the $^{28}Si^-$ signal was used to help identify the biogenic silica. The other ions ($^{12}C^-$, $^{12}C^{14}N^-$, and $^{32}S^-$) were used to check the presence of organic matter. Measurements were conducted over several measuring sessions and in random order of samples.

NanoSIMS data were processed with an updated version of the Matlab-based freeware software Look@NanoSIMS (Polerecky et al., 2012). The general approach involved the quantification of ^{18}O atom fractions in manually drawn regions of interest (ROIs), and their variation with depth (measurement plane) in the sample (see details in Supplementary Methods). The ROI-specific ^{18}O atom fraction, $x(^{18}O)$, was calculated from the secondary ion counts accumulated over the ROI pixels as $^{18}O/(^{16}O+^{18}O)$. The negligible contribution of the isotope ^{17}O was not considered.

2.4. Raman spectroscopy

Raman spectrometry was used to identify the molecular structure of the biogenic silica. Analysis was performed with a WITec Alpha 300R Raman spectrometer using the 532 nm line generated by a Nd-YAG laser. The instrument is equipped with an optical microscope and a 100 × objective lens (numerical aperture of 0.8) allowing measurements with a lateral resolution of ~1 μm and depth resolution of slightly larger than 1 μm. A grating of 600 grooves/mm was used to obtain the entire spectral region of interest (100–3700 cm^{-1}) in a single spectrum allowing direct comparison of bands in different regions. Signal to noise ratio was improved by taking each spectrum for five seconds and averaging over 10 acquisitions. Background removal was performed using the WITec Project Plus software (version 4), and band fitting was conducted in Fityk (Wojdyr, 2010).

For the spicules incubated in ^{18}O-enriched water for two weeks, Raman measurements were performed in 1D (depth scans; same x and y position, increasing z) and 2D (same y position, varying x and z positions). Only depth scans were performed for the control spicule and quartz. For comparison, a fossil frustule (~50 μm diameter), was also targeted for spectral analysis to determine water content. Fresh diatom samples were significantly smaller and thinner and could therefore not be studied because the depth resolution of the Raman spectroscopy (~1 μm) exceeds the thickness of the frustule valves, which is for *T. pseudonana* in the range 63–150 nm (Hildebrand et al., 2006).

3. RESULTS

3.1. ^{18}O-enrichment in biogenic amorphous silica vs. crystalline silica

After two weeks of incubation in ^{18}O-enriched seawater, biogenic silica samples showed significant enrichment in ^{18}O compared with the controls (Fig. 1). In contrast, no significant differences were detected for the crystalline silica samples ($p > 0.05$; Tables S1–3). Of the biogenic silica samples, the ^{18}O enrichment was lowest in the sponge spicules ($x(^{18}O) \approx 2.8 \times 10^{-3}$) while it was quite substantial for the fresh diatom frustules ($x(^{18}O) \approx 26 \times 10^{-3}$). Fossil diatom frustules also showed significant enrichment ($x(^{18}O) \approx 3.6 \times 10^{-3}$). No significant differences were observed for enriched spicules that were remeasured after having spent three months in the vacuum (10^{-9} mbar) of the vessel chamber of the NanoSIMS instrument (data not shown). Repeated measurements of the very same frustules were not possible as each frustule was completely sputtered away during the nanoSIMS measurement.

3.2. Rapid post-mortem increase in ^{18}O-enrichment in diatom frustules

Diatom frustules incubated in ^{18}O-enriched seawater at 15 °C showed rapidly increasing ^{18}O atom fractions, but the exchange rate gradually decreased with time (Fig. 2). No significant differences were observed between the natural and autoclaved seawater samples at any time point measured (Fig. S3).

Images revealed that $x(^{18}O)$ in the frustule valve was significantly larger than in the girdle (Fig. 3). The distribution of $x(^{18}O)$ was generally homogenous within the valve, both in the lateral and vertical dimensions (Fig. S2). Although the studied species have very similar morphology, but

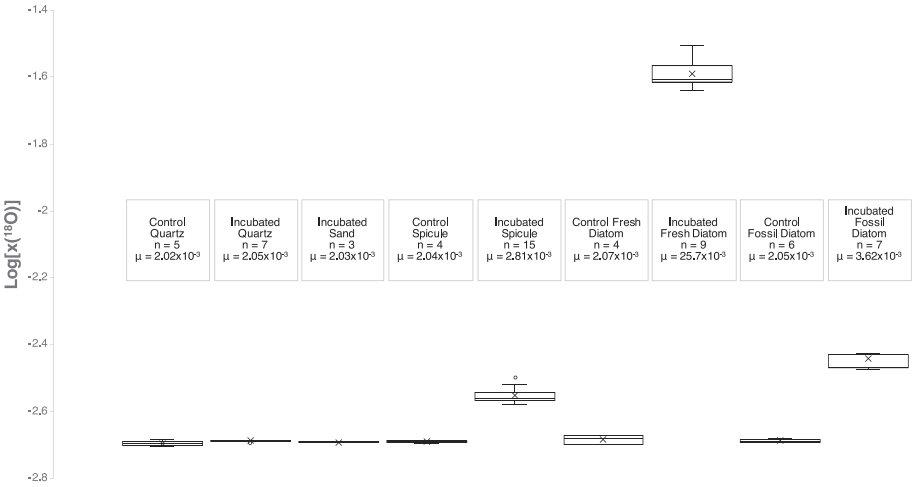

Fig. 1. ^{18}O atom fractions in various forms of silica. A comparison is made between control samples with samples incubated for 2 weeks in ^{18}O-enriched seawater ($x(^{18}O) \approx 0.09$). Data-points correspond to average $x(^{18}O)$ for individual specimens measured for each sample type. Data are presented on a logarithmic scale in a Box-Whisker plot. The number of observations (n), mean value (μ and 'x' in the box) and whiskers of 1.5 inter-quartile ranges are presented. The data was collected over several measuring sessions and in random order of samples to confirm reproducibility of the measurements.

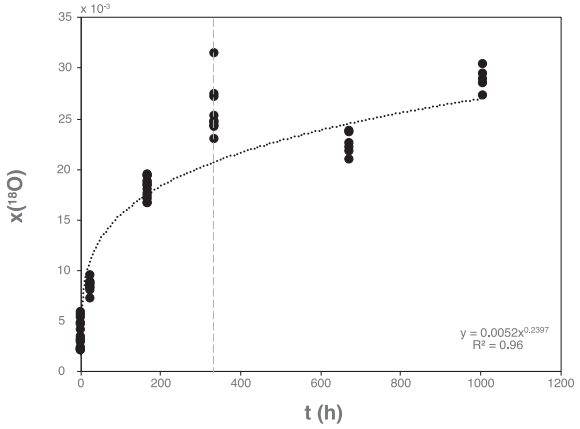

Fig. 2. Time-evolution of the post-mortem ^{18}O atom fractions in diatom frustules at 15 °C. Dashed line indicates the 2-week mark. Trend is fitted with a power function. Data-points correspond to average $x(^{18}O)$ for individual frustules. The dataset contains all the measured diatom samples including control frustules (data-points at $t = 0$), and frustules incubated in ^{18}O-enriched seawater that was or was not autoclaved (distinction between these two treatments is shown in Fig. S3).

slightly different frustule diameters (*T. pseudonana*: 4–7 μm; *T. weisflogii*: 7–10 μm), the differences in frustule diameter had no apparent effect on the measured $x(^{18}O)$ (Fig. S4).

Incubations in ^{18}O-enriched seawater for 2 weeks revealed that frustules incubated at 4 °C had a significantly lower $x(^{18}O)$ than the frustules incubated at 15 °C (Fig. 4). However, both were significantly enriched compared to the control samples ($\sim 2 \times 10^{-3}$). Using the Arrhenius equation and the measurements at these two temperature-points, the activation energy was estimated as $E_a = 30.9 \pm 4.6$ kJ mol^{-1} K^{-1}.

3.3. ^{18}O-enrichment in sponge spicules

Similar to diatom frustules, ^{18}O atom fractions in sponge spicules incubated in ^{18}O-enriched seawater showed a clear increase over time (Fig. 5). The variability among specimens also increased with time (Fig. 5). However, at the same temperature (15 °C) and after the same incubation time (2 weeks) the average $x(^{18}O)$ in the spicules (2.84×10^{-3}) was significantly lower than in the diatom frustules (25.7×10^{-3}; Fig. 1).

The distribution of $x(^{18}O)$ in the spicules was mostly homogeneous throughout the silica structure (Fig. 6). Occasionally, a locally increased ^{18}O enrichment was observed in areas of 0.5–1 μm in size along the edges of the spicule (Fig. 6a), but there were no differences between these areas and the rest of the spicule apparent in the SEM images. In several spicules, a depression (axial canal) running through the spicule was observed (Fig. 6d). This axial canal contained markedly higher amounts of S (Fig. S5) and was slightly more enriched in ^{18}O than the rest of the spicule silica (Fig. 6e–f).

3.4. Raman spectroscopy of amorphous and crystalline silica

While nanoSIMS provides information on the distribution of oxygen isotopes, it does not provide information on the molecular structures in which the oxygen atoms are present. Raman spectroscopy, however, can distinguish these forms and may provide information about which of the potential O-bearing pools in the silica may have been contributing to the observed ^{18}O-enrichment.

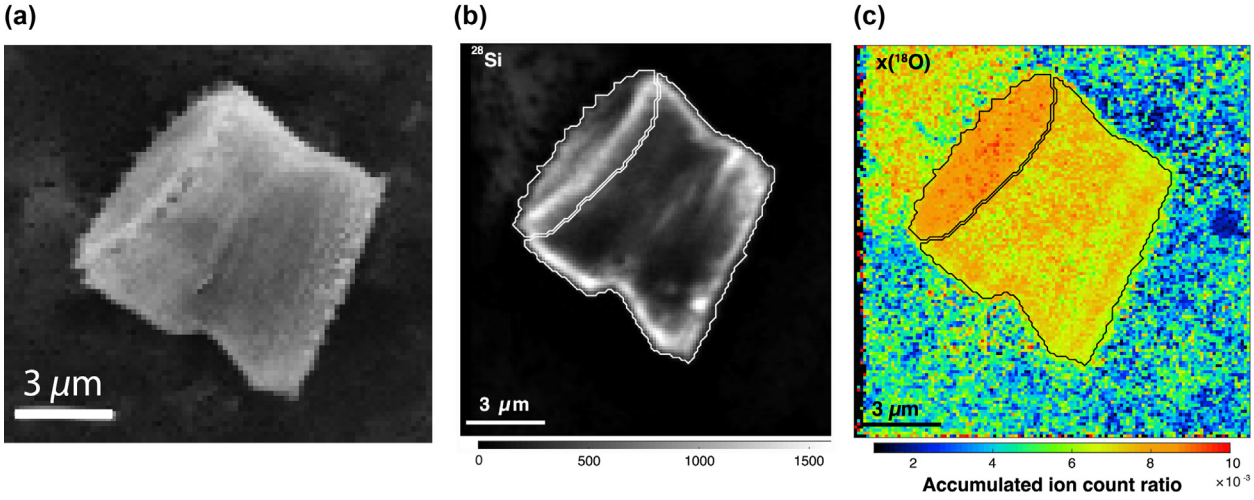

Fig. 3. Distribution of the ^{18}O atom fraction in a diatom frustule. Shown are representative images of an intact frustule incubated in ^{18}O-enriched seawater for 24 h. (a) SEM image. (b) Accumulated ^{28}Si ion count image. White lines mark the valve and the girdle. (c) Image of the ^{18}O atom fraction showing relatively greater enrichment in the valve (8.3×10^{-3}) compared to the girdle (7.1×10^{-3}). Note the apparent increase in x(^{18}O) around the frustule, which is likely caused by redeposition of ^{18}O atoms sputtered from the frustule onto the underlying substrate during the nanoSIMS measurement.

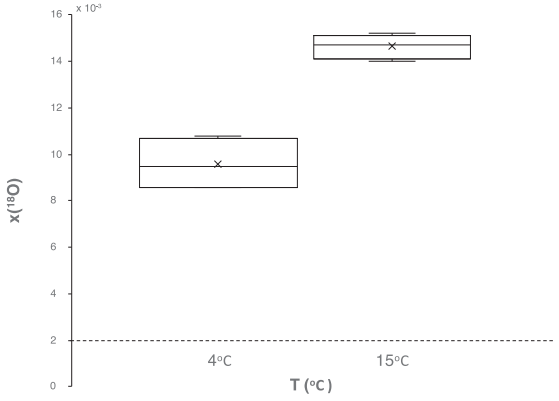

Fig. 4. ^{18}O atom fractions in diatom frustules incubated for 2 weeks in ^{18}O-enriched seawater at different temperatures. Dashed line represents the ^{18}O atom fraction in the control samples ($\sim 2 \times 10^{-3}$). 'x' = mean values and whiskers show 1.5 × IQR. Note that the starting conditions were different from the experiment in Fig. 2 (see Section 2.2).

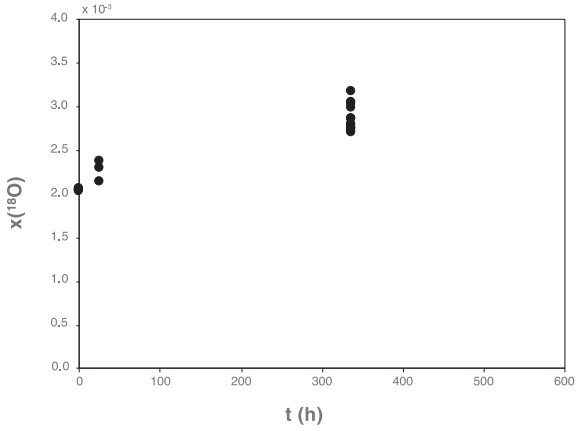

Fig. 5. Time-evolution of ^{18}O atom fractions in sponge spicules incubated in ^{18}O-enriched seawater at 15°C. Datapoints correspond to the average x(^{18}O) for individual spicules.

A distinct feature in the Raman spectra of the sponge spicules (amorphous structure) is the band around 975 cm^{-1}, which is absent in the Raman spectra of quartz (crystalline structure) (Fig. 7a). This band was attributed to the Si-O stretching associated with the silanol group (De Tommasi et al., 2018, and references therein). The presence of this group was further confirmed by the sharp band in the region around 3610 cm^{-1}, which is characteristic for the stretching of the O-H bond associated with silanol groups rather than in liquid water (Kammer et al. 2010). The [$Si\text{-}O\text{-}Si_{790cm\text{-}1}$/$Si\text{-}OH_{975cm\text{-}1}$] band ratio (Fig. 7a) did not vary between the control spicule and the spicule incubated in ^{18}O-enriched water. The presence of -OH is one of the distinguishing characteristics of amorphous silica, as these groups cannot be present in crystalline silica due to the orderly and tightly packed atomic structure. The distribution of the silanol –OH group within sponge spicules was also studied, but no spatial patterns were detected, potentially due to the lower spatial resolution of the Raman measurements in comparison to the nanoSIMS (Fig. S6).

Another distinctive feature in the Raman spectra of the sponge spicules was the broad water band around 3400 cm^{-1}. Both the spicules and quartz used for measurements shown in Fig. 7a did not spend time in a vacuum. In order to check if water signals were the source of the ^{18}O-enrichment observed in the nanoSIMS measurements, measurements were performed on samples that had spent five days in a vacuum (10^{-8} mbar). The measurements

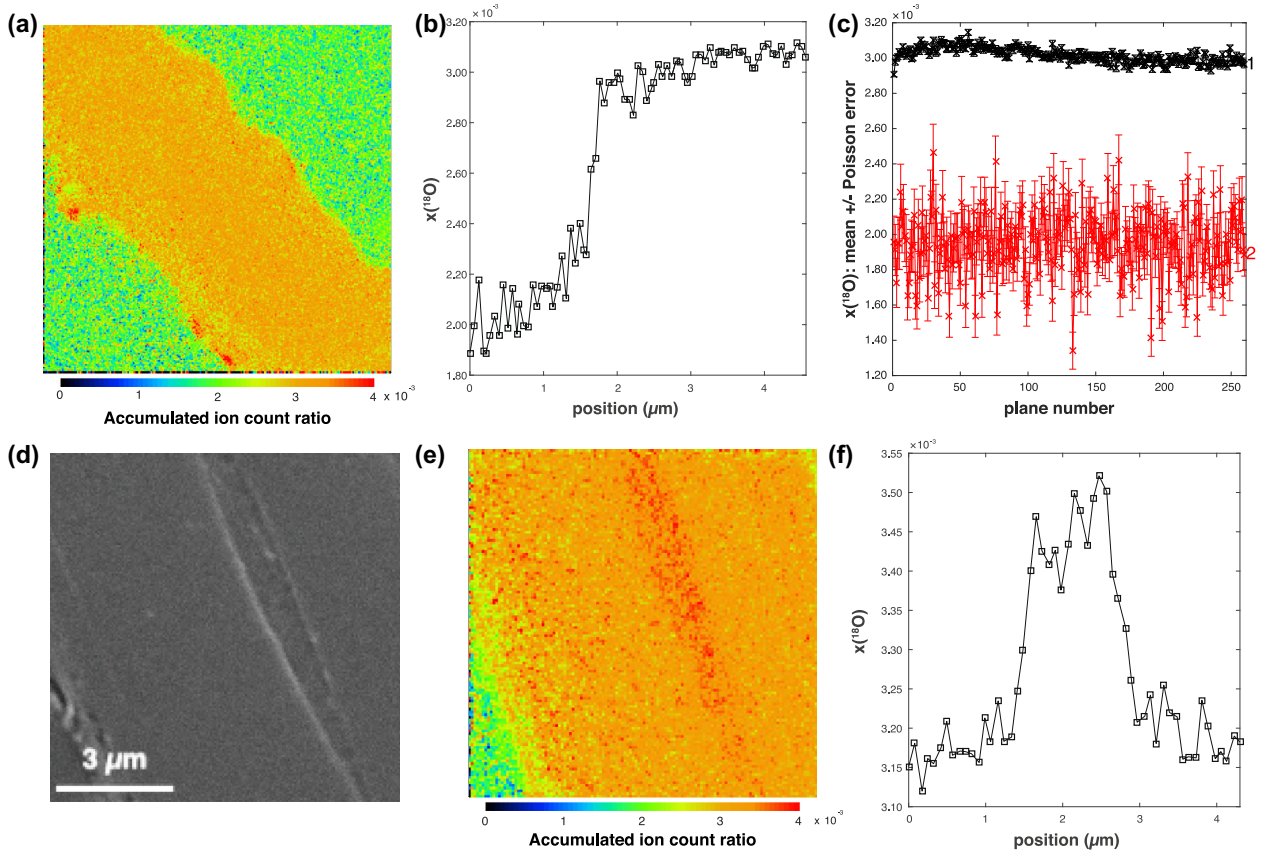

Fig. 6. Distributions of ^{18}O atom fractions in sponge spicules incubated in ^{18}O-enriched seawater for 2 weeks. (a) Image showing the distribution of ^{18}O atom fractions in a spicule cross-section. (b) Lateral profile of ^{18}O atom fraction along a line shown in panel (a). (c) Depth profile of the ^{18}O atom fraction in the spicule (black) and in the resin (red). (d) SEM image of another spicule showing a depression identified as the axial canal. (e) Image of the ^{18}O atom fraction in the spicule shown in panel (d). (f) Lateral profile of the ^{18}O atom fraction along a line shown in panel (e). (For interpretation of the references to colour in this figure legend, the reader is referred to the web version of this article.)

Table 1
Raman band assignments. Identification was based on (McMillan et al., 1982; Terpstra et al., 1990; Kammer et al., 2010; De Tommasi et al., 2018).

Band position (cm^{-1})	Band assignments
(a) 460–490	Si-O-Si stretching
(b) 768–848	Inter tetrahedral Si-O-Si
(c) 945–1010	Si-OH stretching
(d) 1020–1134	Si-O-Si network
(e) 3590–3610	-OH stretching of Si-OH groups
3000–3700	Region with -OH stretching in the water molecule

showed that the spectrum for spicule did not change (data not shown), meaning that the water signal was still present. However, we also analyzed a fossil diatom frustule that had been incubated in ^{18}O-seawater. The frustule was significantly enriched in ^{18}O ($x(^{18}O) = 3.57 \times 10^{-3}$), but the Raman water signals were absent (Fig. 7b).

3.5. Influence of heating under vacuum on the ^{18}O atom fraction in sponge spicules

Since the Raman measurements showed the presence of water in the silica structure after five days in a vacuum, the spicules previously measured by nanoSIMS were heated for additional 7 hours in a vacuum of the NanoSIMS airlock (10^{-8} mbar) and remeasured. The exact temperature could not be determined but was estimated to be higher than 80 °C. This treatment increased the mean ^{18}O atom fraction from 2.83×10^{-3} to 2.93×10^{-3} (Fig. 8), but the increase was not statistically significant ($p > 0.05$; Supplementary Tables S4 and S5).

4. DISCUSSION

This study revealed that biogenic silica undergoes rapid resetting of the O-isotope signature when incubated in ^{18}O-enriched water. Moreover, the exchange appears to

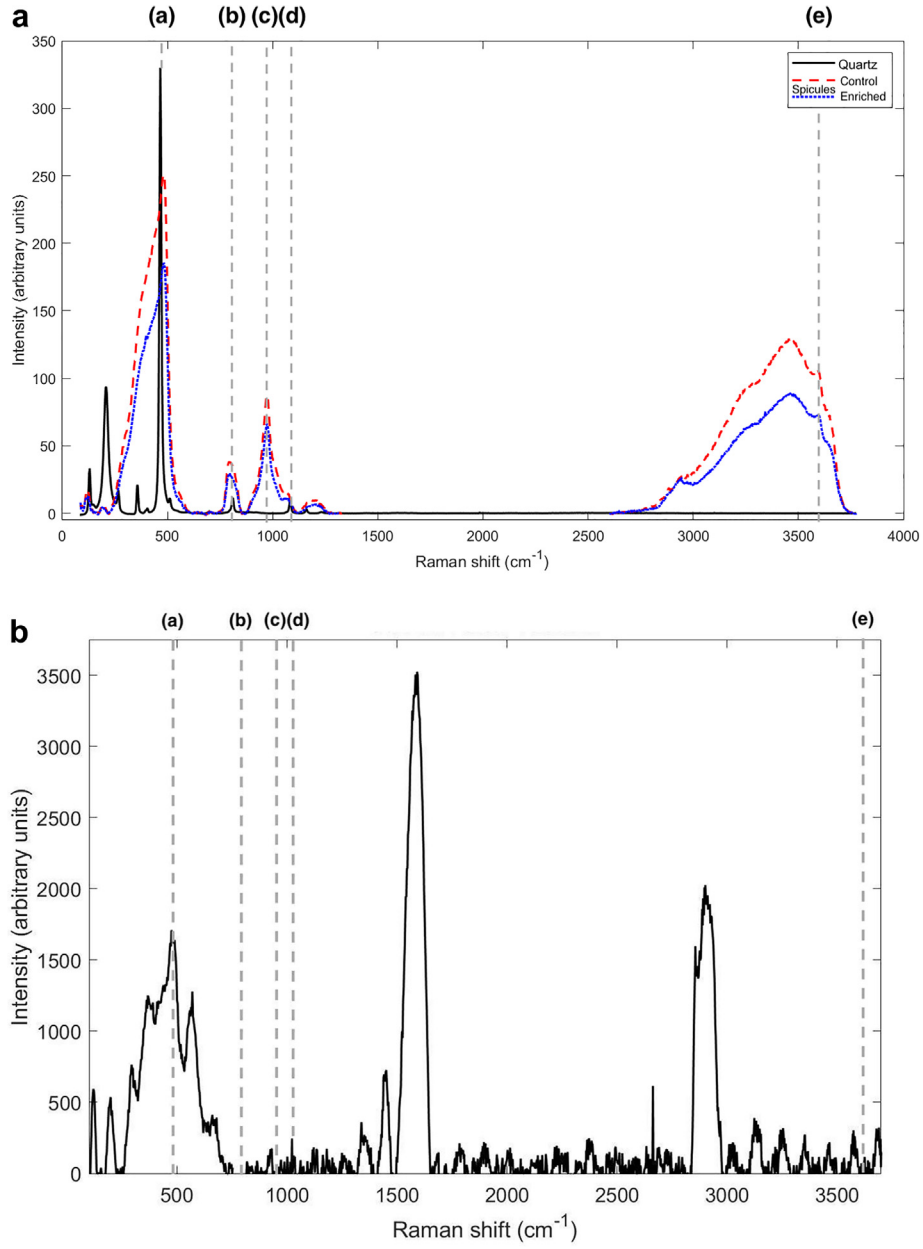

Fig. 7. Raman spectra from sponge spicules, quartz and fossil diatom frustule. Identities of the target bands are listed in Table 1. (a) Spicules and quartz. The spicule (blue line) and quartz (black line) were incubated in ^{18}O-enriched seawater for 2 weeks. Red line corresponds to the control spicule. (b) Fossil diatom frustule. The frustule was incubated for two weeks in ^{18}O-enriched seawater, and subsequently stored for five days in a vacuum (10^{-9} mbar) to remove any residual adsorbed water. Strong signals for ∂C-Hx (1364–1438 cm^{-1}) and υC-Hx (2826–3021 cm^{-1}) are visible in the spectrum but are not marked for this study. The frustule was significantly enriched in ^{18}O (x(^{18}O) = 3.57 × 10^{-3}). (For interpretation of the references to colour in this figure legend, the reader is referred to the web version of this article.)

take place not only for the surface silanol groups, but also for the internal silanol groups which may have consequences for the rest of the silica matrix. This confirms concerns that have been raised regarding the role of post-mortem maturation in influencing δ^{18}O of fossil diatom frustules. While previous research has focused on diagenesis in the sediment, this study shows that oxygen isotope exchange can already take place in the water column. By comparing different forms of biogenic amorphous silica and crystalline silica, the significance of the isotope exchange in biogenic silica becomes clear and hypotheses can be formulated about its impact under natural conditions.

4.1. Post-mortem oxygen exchange in amorphous biogenic silica

In the case of diatom frustules, their susceptibility to post-mortem oxygen exchange becomes evident from the rapid changes in their ^{18}O atom fractions with time. After

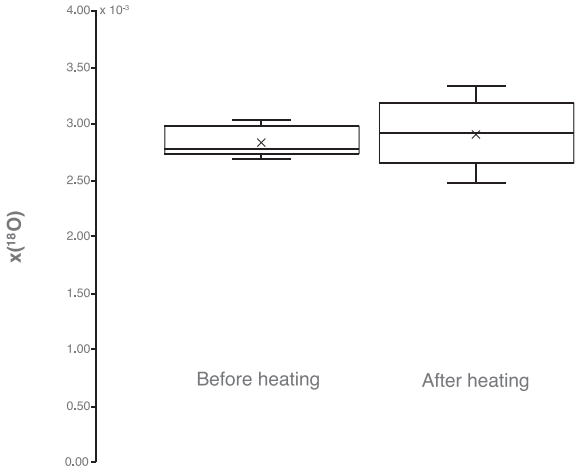

Fig. 8. ^{18}O atom fractions of spicules before and after heating under vacuum. Data represents measurements from the same individual spicules (n = 7). 'x' = mean values and whiskers show 1.5 × IQR.

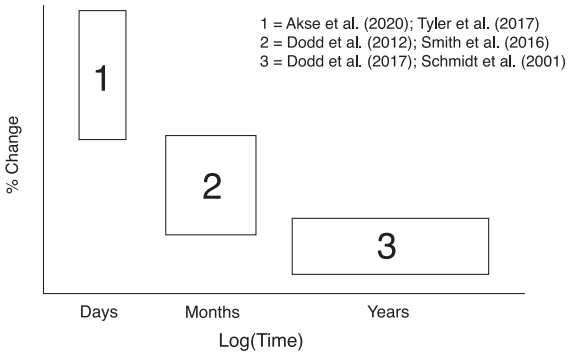

Fig. 9. Schematic diagram showing how this study is placed in a context of other studies investigating post-mortem overprinting of frustule $\delta^{18}O$.

spending only 24 hours in the ^{18}O-enriched seawater (x(^{18}O) ≈ 0.09), we already observed significant changes, while after one week the frustules displayed ^{18}O atom fractions that are an order of magnitude higher compared to the controls. After six weeks the ^{18}O atom fraction reached around 0.029, which was about a third of the ^{18}O atom fraction in the incubation water. This study thus confirms earlier work that also showed similar alterations on the timescale of days to weeks (Tyler et al., 2017).

In this study, the rate of change of $x(^{18}O)_{frustule}$ decreases over time, likely in part due to the decreasing difference between the ^{18}O atom fraction of the water and the frustule and the increasing dissolved Si concentrations (Fig. S1). Over longer timescales a decrease in reactivity is also expected due to other processes. In sediment samples decreasing reactivity is often attributed to the diminishing number of silanol groups by silica maturation (Dodd et al., 2012; Schmidt et al., 2001; Moschen et al., 2006; Lewin, 1961; Brandriss et al., 1998, among others). Despite the decreasing reactivity, the impact over geological timescales can be substantial. This decreasing, but persistent, reactivity was also acknowledged by Dodd et al. (2017), who mentioned that "the dehydroxylation process has the potential to continue to alter $\delta^{18}O$ values for ~10^4–10^6 years." Qualitatively, our results can be placed in the context of other studies investigating post-mortem overprinting of frustule $\delta^{18}O$ as shown in Fig. 9.

A potential inhibitor of post-mortem oxygen transfer in the water column is the presence of a protective organic membrane surrounding the frustule (Moschen et al., 2006). Indeed, the presence of the organic membrane has been shown to strongly reduce biogenic silica dissolution rates, confirming its protective nature when not strongly altered by the presence of bacteria (Bidle and Azam, 1999, 2001). Observations of varying $\delta^{18}O$ in settling diatom detritus in a lacustrine environment have been attributed to resuspended sedimentary frustules affecting the deep trap rather than rapid oxygen exchange affecting the frustules in the water column (Moschen et al., 2006). In an attempt to assess the role of the protective organic membrane in inhibiting secondary oxygen exchange, experiments in this study were performed with both natural seawater (biotic) as well as autoclaved seawater (abiotic). By autoclaving the water, the bacterial population should be minimized, preventing attacks on the organic membrane, leaving it intact. The ensuing data showed no significant differences in dissolution (Fig. S1) or ^{18}O-exchange (Fig. S3) between the two treatments, suggesting that the natural seawater experiment likely also had very little bacterial activity. The observed ^{18}O-enrichment in the frustules incubated in autoclaved water suggests that post-mortem oxygen exchange is possible despite the potential presence of a protective membrane.

Instead of dissolution, the hydrous Si-OH layer is seen as the main contributor to the differences observed in $\delta^{18}O_{frustule}$ of surface-water diatoms and those found in the sediment (e.g. Brandriss et al., 1998; Moschen et al., 2005; Dodd and Sharp 2010). Though the diatom data in this study clearly confirm the post-mortem interaction of diatom frustules with their surrounding waters, the porous and relatively thin morphology of the frustules makes it challenging to determine whether surface silanol groups and tetrahedrally bonded silica were similarly altered. Therefore, the experiment was repeated with siliceous sponge spicules, which have a comparable amorphous silica matrix but a thicker and larger physical structure (e.g. Gendron-Badou et al., 2003), providing more material for nanoSIMS measurements.

Similar to the diatom samples, spicules incubated in ^{18}O-enriched seawater displayed increased ^{18}O atom fractions. The 2-week incubated spicules showed an increase in $x(^{18}O)$ from ~2×10^{-3} to ~3×10^{-3} (Fig. 5). Some spicules were remeasured after spending three months in a vacuum (10^{-9} mbar) at 20 °C, while others were remeasured after spending 7 hours in a vacuum (10^{-8} mbar) under increased temperatures (>80 °C). These spicules showed reproducible values, suggesting that adsorbed water was sufficiently removed for all measurements and did not play a role in the observed ^{18}O-enrichment. Instead, it appears that entire spicule can become enriched with ^{18}O in a matter of several days. Compared to diatom frustules, the rate of

exchange is lower in spicules, probably due to the reduced surface area. Unfortunately, the exact rate cannot be obtained from the present experiment. To determine this, unknowns such as the reactive surface area and silanol abundance need to be constrained, which is outside the scope of this manuscript. The increasing variability of values as time progresses further demonstrates the need to constrain these uncertainties in future work.

4.2. Oxygen exchange in crystalline silica

By measuring additional forms of silica, it became clear that, unlike the biogenic amorphous silica of sponge spicules and diatom frustules, crystalline silica was not affected by ^{18}O exchange. Neither quartz crystals nor sand grains showed changes in their ^{18}O atom fractions after spending time in the ^{18}O-enriched water. This is an important observation for multiple reasons. First, these results confirm that the elevated ^{18}O atom fractions in the embedded and polished spicules cannot be attributed to sample preparation, as the same methodology was used for the crystalline silica. Second, it means that the secondary exchange of oxygen on the timescale of weeks is a phenomenon reserved for biogenic amorphous silica. With this interpretation, it should be kept in mind that the crystalline nature and size of the tests would have influenced the surface area and thus amount of available reactive sites in contact with the ^{18}O-enriched seawater.

4.3. Distribution of ^{18}O in biogenic amorphous silica

For the $\delta^{18}O$ proxy in biogenic silica, it is vital that we further understand the effect of post-mortem processes. Therefore, the chemistry of the individual tests was studied at a sub-micron level. In this way, it was possible to determine whether the oxygen exchange only took place at local hotspots, as a surface deposit or throughout the entire silica structure.

4.3.1. Diatom frustules

Our analyses showed a uniform distribution of the ^{18}O atom fraction throughout the diatom valve. This was clear from both the homogenous lateral distribution in the $x(^{18}O)$ image (Fig. 3c, Fig. S2f) as well as from the stable depth profile of $x(^{18}O)$ through the frustule silica, where the high $x(^{18}O)$ values persisted as long as the frustule silica was detected (Fig. S2d). The decrease in $x(^{18}O)$ with depth was observed not because the frustule material was less enriched in ^{18}O, but because of an increasing interference from the underlying substrate as the thin frustule was sputtered away (Fig. S2). Laterally, the diatom girdles were less enriched in ^{18}O than the valves (Fig. 3), but as only valves are commonly represented in the sediment archive, these were the focus of this study. Our NanoSIMS data from the diatom frustules could not conclusively distinguish between the enrichment of the silanol groups and a possible enrichment of the tetrahedrally bonded oxygen. What they do tell us, however, is that the oxygen in the ambient water molecules can similarly affect both the external silanols as well as the internal silanols (Loucaides et al., 2010).

This is of importance as studies have shown that internal silanol groups may be more abundant than external silanols, as well as more difficult to remove with the current dehydroxylation techniques (e.g., Dodd et al. 2017). Furthermore, as studies have suggested that the condensation of Si-OH groups might be responsible for $\delta^{18}O_{diatom}$ changes during maturation (e.g., Dodd et al., 2017; Schmidt et al., 2001), infiltrating secondary oxygen could become part of the silica matrix throughout the frustule (Fig. 10). So even though the presence of an organic membrane encompassing the frustule prevents rapid dissolution (Bidle and Azam, 1999), a small amount of infiltrating water can start this reaction. This suggests that current dehydroxylation techniques are not sufficient to remove the entire secondary oxygen signal.

4.3.2. Sponge spicules

Generally, the measured spicules showed relatively homogenous ^{18}O atom fractions throughout. Variations only occurred in the axial canal and as small hotspots at the edge between the spicule and the resin. The source of the hotspots could not be determined, but these were not consistently present throughout the measurements. The presence of enriched surface silanol groups seemed to be confirmed by the elevated ^{18}O atom fractions observed in the axial canals. The labeled water was likely able to invade the axial canal and exchange oxygen with the -OH groups. Similar to the ^{18}O signal, the ^{32}S signal was also elevated in the axial canal (Fig. 6 and Fig. S5). A similar observation was previously made in calcareous sponge spicules (Kopp et al., 2011), where the detected S was attributed to the presence of sulphated polysaccharides embedded in the organic matrix of the biomineral. It is possible that the presence of proteins enhanced the uptake of secondary oxygen. However, it is more likely that the observed ^{18}O enrich-

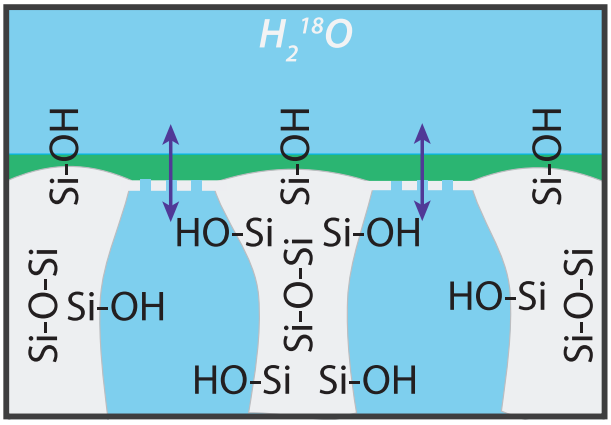

Fig. 10. Schematic diagram of oxygen exchange between the diatom frustule and ambient water. Despite the presence of an organic membrane (green) surrounding the frustule silica (grey), ^{18}O enriched water infiltrates into the frustule pores leading to exchange of oxygen with internal silanols. (For interpretation of the references to colour in this figure legend, the reader is referred to the web version of this article.)

ment was a result of the presence of surface silanols. These observations imply two active processes: the swift oxygen exchange and condensation of labile hydroxyl groups followed by a slower diffusion of oxygen into the rest of the opal matrix.

4.4. Raman measurements on amorphous and crystalline silica

A significant result from the Raman measurements was the reproducibility of the data among the different spicules, meaning that the observed isotope exchange was not related to a physical phase change such as recrystallisation. Moreover, according to the Raman measurements, the main distinguishing feature of the spicule relative to the quartz was the presence of Si-OH, which suggests that oxygen isotope exchange in biogenic silica is enabled by the presence of silanol groups. Moreover, the more open nature of the amorphous silica structure facilitates diffusion of water and consequently oxygen exchange. The open nature of amorphous silica is confirmed by the enrichment observed in the fossil diatom frustule despite the absence of signals due to Si-OH (Fig. 7b). Thus, the availability of reactive sites and the open amorphous structure of biogenic silica allow the post-mortem overprinting of oxygen signal in the entire silica matrix.

4.5. The potential sources of oxygen signal

The nanoSIMS results show a homogenous distribution of x(^{18}O) through the amorphous silica structures of the diatom frustules and sponge spicules. However, the nanoSIMS does not provide information on the structural site in which the oxygen atom is located. Within the silica, there are four potential O-bearing pools: (1) water adsorbed to the silica, (2) water trapped within the silica architecture, (3) silanol (Si-OH) units (Knauth and Epstein, 1982) and (4) siloxane (Si-O-Si) within the silica structure.

The first pool, loosely adsorbed water, is removed before measurement by initial drying of the samples in air as well as by degassing in the vacuum chambers of the nanoSIMS instrument. Therefore, it is unlikely that this pool contributed to the measured signal. Determining the relative contribution of the other three pools (water trapped in the silica structure, siloxane and silanol) is more challenging as the Raman measurements of the spicules show that all three are present within the structure (Fig. 7) even after exposure to the nanoSIMS vacuum for five days. Considering that the estimated activation energy of ^{18}O exchange in diatoms ($\sim$31 kJ mol^{-1} K^{-1}) was higher than the activation energy of self-diffusion of free liquid water ($\sim$19 kJ mol^{-1} K^{-1}; Mills, 1973; Fripiat et al., 1984), it is likely that water entered the structure. Water might be present in the ultramicropores (size $<$ 1 nm) and in the OH groups that are located at the walls of these pores, classified as internal silanols (Zhuravlev, 2000; Sato et al., 2011). Together with external silanol groups, these pools account for 6–10 wt% of the total oxygen content in frustules found in the sediment (Chapligin et al., 2011). The remaining $\sim$90% can be attributed to oxygen in siloxane groups (Si-O-Si). For fresh biogenic silica, the relative silanol abundance is likely greater as shown by calculated ratios between tetrahedrally bonded silica (Q4) and hydroxyl-bound oxygen within hydrated silica ($Q_{1\text{-}3}$ referred to as Q3), which range between 1.5 and 2 for fresh diatoms and spicules (Gendron-Badou et al., 2003).

Considering the magnitude of the ^{18}O atom fraction observed in the diatom frustules (reaching $\sim$30% of the ^{18}O atom fraction of the incubation seawater), and the relative contribution of silanol groups to the total O pool, our results suggest that oxygen in both the internal and external silanols is altered due to the secondary oxygen exchange with the surrounding water.

In the spicules, the presence of internal water in the silica matrix (even after having spent several days in the vacuum) is undeniable and this could contribute to the ^{18}O-enrichment. However, it is unlikely that this pool contributed significantly to the ^{18}O-enrichment observed by nanoSIMS. Firstly, fossil diatom frustules incubated in ^{18}O-enriched water for 2 weeks showed higher ^{18}O enrichment than spicules, but Raman spectroscopy did not detect any water in these samples (Fig. 7b).

Secondly, ^{18}O atom fraction measured by nanoSIMS increased with the exposure time of the samples to the ^{18}O-enriched water (Figs. 2 and 5). The lack of a diffusion profile across the spicule samples indicates that diffusion into the pores was efficient on the timescale of the experiments. In fact, the depth profiles of fresh frustules revealed very rapid diffusion due to a very brief (minutes) exposure to MilliQ. This hints at the efficiency to which the water diffuses into the structure. Therefore, if water in the pores had a significant contribution, the ^{18}O atom fractions measured by nanoSIMS would be stable, rather than increasing with time.

Lastly, volatilization of water through heating to $\sim$ 100 °C has been found to occur without isotopic exchange with silica-bound oxygen (Labeyrie, 1974). Therefore, it is unlikely that the water signature can give rise to the ^{18}O/^{16}O signatures through exchange during sample pretreatment for nanoSIMS analysis. Indeed, even additional heating of the spicules under vacuum in the nanoSIMS airlock did not result in significantly lower ^{18}O atom fractions (Fig. 8).

Water within the diatoms appears to be removed easier than from the spicules. Frustules will therefore likely contain less water, probably due to their thinner and more open architecture. If water was indeed removed from the frustules, only the silanol and siloxane groups would remain. Moreover, the presence of structurally bound water may actually aid the diffusion processes of oxygen into the silica structure by providing an internal pool directly influenced by the external water signature with which internal silanols can exchange.

4.6. Secondary oxygen exchange under natural conditions

Our experiments used highly enriched seawater (^{18}O atom fraction of $\sim$9%) to estimate the rate of ^{18}O exchange in biogenic silica. Considering that diatom frustules may spend around 2–4 weeks in the water column

before reaching the seafloor, and assuming a natural $\delta^{18}O$ gradient in the marine water column of ~3‰, the change in the $\delta^{18}O_{diatom}$ would likely be within a typical analytical error margin (<1‰), but would nevertheless start deviating from the value determined during the biomineralization phase.

However, several features in the present data raise a concern that, over geological timescales, the alteration may be significant. Firstly, ^{18}O-exchange is more rapid than previously thought, indicating pronounced susceptibility of the oxygen in the frustule to changes in the surrounding water. The moment a frustule starts sinking, secondary oxygen exchange starts, and this continues while the frustules are at the sediment–water interface.

Secondly, although the oxygen exchange slows down by silica maturation during diagenesis, it continues because fossil diatom frustules exchanged ^{18}O (Fig. 1). This implies that over longer timescales the $\delta^{18}O$ signature of a frustule will eventually approach the $\delta^{18}O$ of the surrounding pore water.

Thirdly, the data shows that the oxygen in both internal and external silanols can be altered with time. This results in the presence of an internal oxygen pool directly influenced by changes in the external water signature. Studies have shown that this internal pool is abundant and difficult to remove (e.g. Dodd et al., 2017), and that the silanol groups may condensate to form siloxane during maturation (Schmidt et al., 2001; Dodd et al., 2012, 2017; Moschen et al., 2006) or laboratory treatment (Tyler et al., 2017). As maturation is a gradual but steady process, varying water signatures may become incorporated into the silica structure.

5. CONCLUSION

Our data show that the oxygen isotope signal in biogenic amorphous silica can become rapidly overprinted post-mortem, supporting recent concerns in the literature about early maturation effects on $\delta^{18}O_{diatom}$. While these concerns have focused predominantly on sediment diagenesis, we show that post-mortem maturation can already start playing a role in the water column. This hypothesis is based on the observation that two forms of biogenic silica (diatom frustules and sponge spicules), when placed in ^{18}O-enriched seawater, become rapidly enriched in ^{18}O. NanoSIMS analysis of individual frustules showed that this enrichment occurred throughout the structure. This means that, at the very least, both external and internal silanol groups are similarly affected. Additional mapping of sponge spicules revealed that, despite the more solid structure of the spicules, the entire silica matrix was enriched in ^{18}O, albeit to a lesser degree than the porous diatom frustules. Moreover, a similar experiment with crystalline silica (which lack silanol groups) did not lead to enrichment in ^{18}O. These experiments confirm that the presence of surface silanol groups can lead to a rapid exchange of oxygen between biogenic silica and the ambient water. However, the experiments also revealed that the internal silanol groups are equally effected. As the internal silanol groups are not easily removed, subsequent maturation processes (such as silanol condensation) may result in an altered ^{18}O signature of the siloxane. This implies that despite the current dehydroxylation methods (see Chapligin et al., 2011 for a comparative study), the final measured $\delta^{18}O_{diatom}$ from the frustule will most likely represent a mixed signal from the original growing stage, water-column settling, and sediment pore waters. As silica reactivity has been shown to decrease with time (Fig. 9), the oxygen signal may be dominated by early conditions, but continued reactivity on geological timescales cannot be ruled out. Therefore, records may still show large-scale trends, but detailed inferences about environmental conditions should be made with care.

AUTHOR CONTRIBUTIONS

JJM, LP and SA designed the experiments. SA prepared the samples and conducted NanoSIMS analyses. HK performed the Raman analyses. SA and LP performed NanoSIMS data analysis. HK and SA performed the Raman data analyses. SA interpreted the data, prepared the figures and wrote the manuscript text with contributions from all authors.

Declaration of Competing Interest

The authors declare that they have no known competing financial interests or personal relationships that could have appeared to influence the work reported in this paper.

ACKNOWLEDGEMENTS

We would like to thank M. Grego for culturing the diatom frustules, A. de Kluijver and M. C. Bart for providing spicule samples, A. Roepert for providing the quartz samples, H. de Stigter for providing diatom ooze, and M. Kienhuis for analytical support. The NanoSIMS facility at Utrecht University was financed through a large infrastructure grant by the Netherlands Organisation for Scientific Research (NWO) (grant no. 175.010.2009.011). This work was carried out under the programme of the Netherlands Earth System Science Centre (NESSC), financially supported by the Ministry of Education, Culture and Science (OCW) in the Netherlands (grant no. 024.002.001).

APPENDIX A. SUPPLEMENTARY MATERIAL

Supplementary data to this article can be found online at https://doi.org/10.1016/j.gca.2020.06.007.

REFERENCES

Akse S. P. (2020a) *Data belonging to 'Rapid post-mortem oxygen isotope exchange in biogenic silica'; 4TU*. Centre for Research Data, https://doi.org/10.4121/uuid:bce04d86-732a-4d17-971d-f97a8947088e.

Akse S. P. (2020b) *Studying climate signals through microscale chemical variability in diatoms: A high-resolution chemical imaging study of biogenic silica*. Ph.D., thesis Utrecht University, ISBN: 978-90-6266-569-3.

Bidle K. D. and Azam F. (1999) Accelerated dissolution of diatom silica by marine bacterial assemblages. *Nature* **397**, 508–512.

Bidle K. and Azam F. (2001) Bacterial control of silicon regeneration from diatom detritus: Significance of bacterial ectohydrolases and species identity. *Limnol. Oceanogr.* **46**, 1606–1623.

Bidle K. D., Brzezinski M. A., Long R. A., Jones J. L. and Azam F. (2003) Diminished efficiency in the oceanic silica pump caused by bacteria-mediated silica dissolution. *Limnol. Oceanogr.* **48**, 1855–1868.

Brandriss M. E., O'Neil J. R., Edlund M. B. and Stoermer E. F. (1998) Oxygen isotope fractionation between diatomaceous silica and water. *Geochim. Cosmochim. Acta* **62**, 1119–1125.

Chapligin B., Leng M. J., Webb E., Alexandre A., Dodd J. P., Ijiri A., Lücke A., Shemesh A., Abelmann A., Herzschuh U., Longstaffe F. J., Meyer H., Moschen R., Okazaki Y., Rees N. H., Sharp Z. D., Sloane H. J., Sonzogni C., Swann G. E. A., Sylvestre F., Tyler J. J. and Yam R. (2011) Inter- laboratory comparison of oxygen isotope compositions from biogenic silica. *Geochim. Cosmochim. Acta* **75**, 7242–7256.

De Tommasi E., Congestri R., Dardano P., De Luca A. C., Managò S., Rea I. and De Stefano M. (2018) UV-shielding and wavelength conversion by centric diatom nanopatterned frustules. *Sci. Rep.* **8**, 1–14.

Dodd J. P. and Sharp Z. D. (2010) A laser fluorination method for oxygen isotope analysis of biogenic silica and a new oxygen isotope calibration of modern diatoms in freshwater environments. *Geochim. Cosmochim. Acta* **74**, 1381–1390.

Dodd J. P., Sharp Z. D., Fawcett P. J., Brearley A. J. and McCubbin F. M. (2012) Rapid post-mortem maturation of diatom silica oxygen isotope values. *Geochemistry. Geophys. Geosyst.* **13**, 1–12.

Dodd J. P., Wiedenheft W. and Schwartz J. M. (2017) Dehydroxylation and diagenetic variations in diatom oxygen isotope values. *Geochim. Cosmochim. Acta* **199**, 185–195.

Fripiat J. J., Letellier M. and Levitz P. (1984) Interaction of water with clay surfaces. *Philos. Trans. R. Soc. London* **299**, 287–299.

Gendron-Badou A., Coradin T., Maquet J., Fröhlich F. and Livage J. (2003) Spectroscopic characterization of biogenic silica. *J. Non. Cryst. Solids* **316**, 331–337.

Hendry K. R. and Robinson L. F. (2012) The relationship between silicon isotope fractionation in sponges and silicic acid concentration: Modern and core-top studies of biogenic opal. *Geochim. Cosmochim. Acta* **81**, 1–12.

Hendry K. R., Georg R. B., Rickaby R. E. M., Robinson L. F. and Halliday A. N. (2010) Deep ocean nutrients during the Last Glacial Maximum deduced from sponge silicon isotopic compositions. *Earth Planet. Sci. Lett.* **292**, 290–300.

Hendry K. R., Swann G. E. A., Leng M. J., Sloane H. J., Goodwin C., Berman J. and Maldonado M. (2015) Technical Note: Silica stable isotopes and silicification in a carnivorous sponge Asbestopluma sp. *Biogeosciences* **12**, 3489–3498.

Hildebrand M., York E., Kelz J. I., Davis A. K., Frigeri L. G., Allison D. P. and Doktycz M. J. (2006) Nanoscale control of silica morphology and three-dimensional structure during diatom cell wall formation. *J. Mater. Res.* **21**, 2689–2698.

Kammer M., Hedrich R., Ehrlich H., Popp J., Brunner E. and Krafft C. (2010) Spatially resolved determination of the structure and composition of diatom cell walls by Raman and FTIR imaging. *Anal. Bioanal. Chem.* **398**, 509–517.

Knauth L. P. and Epstein S. (1982) The nature of water in hydrous silica. *Am. Mineral.* **67**, 510–520.

Kopp C., Meibom A., Beyssac O., Stolarski J., Djediat S., Szlachetko J. and Domart-Coulon I. (2011) Calcareous sponge biomineralization: Ultrastructural and compositional heterogeneity of spicules in Leuconia johnstoni Carter, 1871. *J. Struct. Biol.* **173**, 99–109.

Labeyrie L. (1974) New approach to surface seawater paleotemperatures using $^{18}O/^{16}O$ ratios in silica diatom frustules. *Nature* **248**, 40–42.

Labeyrie L. and Juillet A. (1982) Oxygen isotope exchangeability of diatom valve silica; interpretation and consequences for paleoclimate studies. *Geochim. Cosmochim. Acta* **46**, 967–975.

Leclerc A. J. and Labeyrie L. (1987) Temperature dependence of the oxygen isotopic fractionation between diatom silica and water. *Earth Planet. Sci. Lett.* **84**, 69–74.

Leng M. J. and Barker P. A. (2006) A review of the oxygen isotope composition of lacustrine diatom silica for palaeoclimate reconstruction. *Earth-Science Rev.* **75**, 5–27.

Lewin J. C. (1961) The dissolution of silica from diatom walls. *Geochim. Cosmochim. Acta* **21**, 182–198.

Loucaides S., Behrends T. and Van C. P. (2010) Reactivity of biogenic silica : Surface versus bulk charge density. *Geochim. Cosmochim. Acta* **74**, 517–530.

Matheney R. K. and Knauth L. P. (1989) Oxygen-isotope fractionation between marine biogenic silica and seawater. *Geochim. Cosmochim. Acta* **53**, 3207–3214.

Matteuzzo M. C., Alexandre A., Varajão A. F. D. C., Volkmer-Ribeiro C., Almeida A. C. S., Varajão C. A. C., Vallet-Coulomb C., Sonzogni C. and Miche H. (2013) Assessing the relationship between the $\delta\ ^{18}O$ signatures of siliceous sponge spicules and water in a tropical lacustrine environment (Minas Gerais, Brazil). *Biogeosci. Discuss.* **10**, 12887–12918.

McMillan P., Piriou B. and Navrotsky A. (1982) A Raman spectroscopic study of glasses along the joins silica-calcium aluminate, silica-sodium aluminate, and silica-potassium aluminate. *Geochim. Cosmochim. Acta* **46**, 2021–2037.

Menicucci A. J., Spero H. J., Matthews J. and Parikh S. J. (2017) Influence of exchangeable oxygen on biogenic silica oxygen isotope data. *Chem. Geol.* **466**, 710–721.

Mills R. (1973) Self-diffusion in normal and heavy water in the range 1–45. *J. Phys. Chem.* **77**, 685–688.

Moschen R., Lücke A. and Schleser G. H. (2005) Sensitivity of biogenic silica oxygen isotopes to changes in surface water temperature and palaeoclimatology. *Geophys. Res. Lett.* **32**, 1–4.

Moschen R., Lücke A., Parplies J., Radtke U. and Schleser G. H. (2006) Transfer and early diagenesis of biogenic silica oxygen isotope signals during settling and sedimentation of diatoms in a temperate freshwater lake (Lake Holzmaar, Germany). *Geochim. Cosmochim. Acta* **70**, 4367–4379.

Müller W. E. G., Li J., Schröder H. C., Qiao L. and Wang X. (2007) The unique skeleton of siliceous sponges (Porifera; Hexactinellida and Demospongiae) that evolved first from the Urmetazoa during the Proterozoic: A review. *Biogeosciences* **4**, 219–232.

Nuñez J., Renslow R., Cliff J. B. and Anderton C. R. (2018) NanoSIMS for biological applications: Current practices and analyses. *Biointerphases* **13**, 03B301.

Polerecky L., Adam B., Milucka J., Musat N., Vagner T. and Kuypers M. M. M. (2012) Look@NanoSIMS - a tool for the analysis of nanoSIMS data in environmental microbiology. *Environ. Microbiol.* **14**, 1009–1023.

Rohling E. J. and Cooke S. (1999) Stable oxygen and carbon isotopes in foraminiferal carbonate shells. In *Modern Foraminifera*. Springer, Dordrecht, pp. 239–258.

Sandford F. (2003) Physical and chemical analysis of the siliceous skeletons in six sponges of two groups (demospongiae and hexactinellida). *Microsc. Res. Tech.* **62**, 336–355.

Sato K., Fujimoto K., Nakata M. and Hatta T. (2011) Diffusion-reaction of water molecules in angstrom pores as basic mechanism of biogenic quartz formation. *J. Phys. Chem. C* **115**, 18131–18135.

Schmidt M., Botz R., Rickert D., Bohrmann G., Hall S. R. and Mann S. (2001) Oxygen isotopes of marine diatoms and

relations to opal-A maturation. *Geochim. Cosmochim. Acta* **65**, 201–211.

Shemesh A., Charles C. D. and Fairbanks R. G. (1992) Oxygen isotopes in biogenic silica: global changes in ocean temperature and isotopic composition. *Science* **256**, 1434–1436.

Smith A. C., Leng M. J., Swann G. E. A., Barker P. A., Mackay A. W., Ryves D. B., Sloane H. J., Chenery S. R. N. and Hems M. (2016) An experiment to assess the effects of diatom dissolution on oxygen isotope ratios. *Rapid Commun. Mass Spectrom.* **30**, 293–300.

Snelling A. M., Swann G. E. A., Pike J. and Leng M. J. (2014) Pliocene diatom and sponge spicule oxygen isotope ratios from the Bering Sea: Isotopic offsets and future directions. *Clim. Past* **10**, 1837–1842.

Swann G. E. A. and Leng M. J. (2009) A review of diatom δ18O in palaeoceanography. *Quat. Sci. Rev.* **28**, 384–398.

Swann G. E. A., Maslin M. A., Leng M. J., Sloane H. J. and Haug G. H. (2006) Diatom δ18O evidence for the development of the modern halocline system in the subarctic northwest Pacific at the onset of major Northern Hemisphere glaciation. *Paleoceanography* **21**, 1–12.

Terpstra P., Combes D. and Zwick A. (1990) Effect of salts on dynamics of water: A Raman spectroscopy study. *J. Chem. Phys.* **92**, 65–70.

Tyler J. J., Sloane H. J., Rickaby R. E. M., Cox E. J. and Leng M. J. (2017) Post-mortem oxygen isotope exchange within cultured diatom silica. *Rapid Commun. Mass Spectrom.* **31**, 1749–1760.

Wojdyr M. (2010) Fityk: a general-purpose peak fitting program. *J. Appl. Crystallogr.* **43**, 1126–1128.

Zachos J. C., Pagani M., Sloan L., Thomas E. and Billups K. (2001) Trends, rhythms, and aberrations in global climate 65 Ma to present. *Science* **292**, 686–693.

Zhuravlev L. T. (2000) The surface chemistry of amorphous silica. Zhuravlev model. *Colloids Surf. A Physicochem. Eng. Asp.* **173**, 1–38.

Associate editor: Anders Meibom